Crystallinity and chain stem length dependence of yield kinetics in polyethylene

Received: 11 May 2022 | Revised: 3 July 2022 | Accepted: 11 July 2022

DOI: 10.1002/pol.20220265

RESEARCH ARTICLE

JOURNAL OF POLYMER SCIENCE WILEY

Crystallinity and chain stem length dependence of yield kinetics in polyethylene

Jevan Furmanski[1] | **Leon Govaert**[2] | **Jonathan Schaefer**[3] | **Joseph A. Throckmorton**[3] | **Johannes A. W. van Dommelen**[2]

[1]Structural Materials Division, University of Dayton Research Institute, Dayton, Ohio, USA

[2]Department of Mechanical Engineering, Eindhoven University of Technology, Eindhoven, Manitoba, The Netherlands

[3]Advanced Characterization Department, ExxonMobil Chemical Company, Baytown, Texas, USA

Correspondence
Jevan Furmanski, Structural Materials Division, University of Dayton Research Institute, Dayton, OH 45469, USA.
Email: jevanf@gmail.com

Funding information
ExxonMobil Research and Engineering Company

Abstract

Researchers have long sought to predict the mechanical behavior of polyethylene from its microstructure. In particular, the yield strength and yield kinetics have been reported to be dependent on crystallinity and crystal thickness, but the relative importance of these two microstructural attributes has not been shown. In the present work, a series of microstructures was obtained through a combination of controlled quench rates from the melt and inclusion of various amounts of hexene comonomer. The yield strength for a wide range of strain-rates was linearly dependent on the crystallinity, and independent of crystal thickness (chain stem length), both measured by Raman spectroscopy. Similarly, yield kinetics described by a Ree-Eyring two-process stress activated model showed linear dependence on crystallinity and no dependence on crystal thickness. The results of the present work call into question models of yield kinetics dependent on screw dislocation nucleation, which depend on crystal thickness.

KEYWORDS

crystal thickness, crystallinity, polyethylene, Raman spectroscopy, stem length, yield kinetics, yield strength

1 | INTRODUCTION

Researchers have long sought to predict the mechanical behavior of polyethylene (PE) from its molecular or microstructural characteristics. The mechanical properties of a wide variety of microstructures of homopolymers and copolymers of polyethylene have been systematically investigated by a number of investigators.[1–5] In these works, the elastic modulus was widely reported to depend directly on the crystallinity, but there was disagreement in these reports on whether the yield strength depends primarily on crystallinity or crystal thickness. This ambiguous correlation of yield strength was complicated by the strong correlation that exists between crystallinity and crystal thickness, potentially rendering them interchangeable. To the authors' knowledge, there has been no attempt yet to determine the yield strength as a function of both crystallinity and crystal thickness, and thus judge their relative contributions.

The yield stress of polyethylene is known to display a marked dependence on applied strain rate and temperature.[1,6] The yield kinetics typically give evidence of the contributions of at least two molecular deformation processes, which results in distinct regimes with different strain rate and temperature dependence of the yield strength. This behavior was modeled using the Ree–Eyring modification[7] of Eyring's activated flow model,[8]

Jevan Furmanski, Leon Govaert and Johannes A. W. van Dommelen contributed equally to this work.

resulting in an accurate prediction of yield strength over a wide range of strain rates and temperatures, and also predicting creep rupture lifetime in the plasticity-controlled regime.[6]

The yield kinetics of polyethylene have been successfully modeled as an activated-rate process,[6] particularly with the objective of predicting the long-term failure of pressurized pipes. These typically consider plasticity as a Ree–Eyring dual-activation mechanism process, which results in two distinct regimes of yield strength dependence on strain-rate.[6–8] These studies were generally conducted at or above room temperature, though others have tested over a wide range of temperatures and a limited range of strain-rates.[1] These models have been successful in fitting a wide range of yield kinetics and also predicting ductile failure lifetimes under constant load.[8]

Plastic deformation in polyethylene crystals is widely attributed to crystallographic slip mechanisms similar to that in metals, mainly building off the dislocation nucleation model proposed by Young[9] and a research working out the energetics of various slip systems in polyethylene.[10] This was conceived in large part to predict the strain-rate and temperature dependence of plasticity in polyethylene from a fundamental mechanism. Young's model derived the critical resolved shear stress for slip based on the energy of the [001] chain axis screw dislocation, which has by far the lowest line energy of any allowable dislocation,[10] and thus the model predicts a crystal thickness dependence of the activation energy for nucleating dislocations and plasticity in general. However, in his original paper on the subject, Young noted that the application of a simple composite model accounts for the yield strength dependence based on crystallinity and the effect of crystal thickness per se may not be consequential.[9] Various other works picked up and expanded on Young's screw dislocation nucleation model,[11–13] all of which consider the yield strength as dependent on crystal thickness and did not directly consider crystallinity, but rather implicitly attributed the yield dependence on crystal thickness only and independent of crystallinity. It should be noted that these works generally report yield as a function of crystal thickness, rather than the more operative chain stem length within the crystal—the chain stems being tilted as some 35 degrees to the surface normal of the crystals.[14–16]

Modeling of the plastic behavior of polyethylene as a semicrystalline composite aggregate has more recently been undertaken, which allows for the accounting of the effects (in principle) of crystallinity, crystal thickness, and crystal orientation distributions.[17–21] In these works, the simultaneous activity of the various slip systems in the crystal phase depends on the relative critical resolved shear stresses for each system. These large-strain micromechanical models of polyethylene deformation have been successful in predicting the evolution of the microstructure with deformation and the attendant development of mechanical anisotropy and crystalline texture. However, while these micromechanical models are based on fine crystallographic slip, they do not explicitly call out the yield kinetics using a dislocation nucleation mechanism as the rate-determining step, but rather utilize a calibration of a thickness-independent slip resistance on each slip system. This represents something of an opportunity, as these models should be fully able to account for both the effect of crystallinity on the overall resistance to deformation in the composite semicrystalline aggregate and the effect of crystal thickness as determining the local slip resistance in a given crystal. To the authors' knowledge, there is no report that considers the potential for a simultaneous effect of both crystallinity and crystal thickness on yield kinetics. The present work was conducted to conclusively determines the simultaneous effect of both crystallinity and crystal thickness on yield kinetics to inform physically predictive micromechanical models of semicrystalline polymers.

2 | MATERIALS AND METHODS

2.1 | Materials and yield stress determination

The strategy of this work was to obtain a wide range of crystallinity and stem lengths by varying crystallization with both undercooling and various concentrations of random short-chain branching. The intent was to use short-chain branching to restrict crystal stem length more directly than that obtainable by controlled undercooling alone in high density polyethylenes (HDPE), and thus enable the decorrelation of stem length from crystallinity as a structural parameter. Only nominal densities above 0.92 g/cc were considered to ensure lamellar microstructures; the micellar microstructures that form at lower densities exhibit predominantly elastomeric behavior and may not show well-behaved crystallographic slip.[22] This approach is nominally similar to that employed by other investigators.[1–5]

All the polyethylenes were gas phase polymerized commercial products chosen as model materials for their narrow molecular weight and comonomer content distributions. All PE employed had a similar weight-averaged molecular weight M_w ~130,000 g/mol. One chrome-catalyzed HDPE was chosen for its relatively low polydispersity, M_w/M_n ~7. Five metallocene-catalyzed hexene comonomer linear-low density polyethylenes (LLDPE) were chosen for their nearly ideal polydispersity, M_w/M_n ~2, and their unusually narrow composition distribution, meaning that the randomly

incorporated hexene comonomer has nearly constant mole fraction for all molecular weight fractions. The nominal densities of the LLDPE resins were 0.920, 0.923, 0.927, 0.935, and 0.940 g/cc.

Compression-molded 0.5 mm thick plaques were crystallized by various cooling conditions: slow-cooling in the press overnight by leaving it under pressure after shutting off the heaters (further referred to as slow-cooled: SC); quenching in the press by water-cooled platens (further referred to as press-cooled: PC); air-cooling on the benchtop (AC); and quenching in an ice bath (IC). The latter two were only applied to the HDPE. Density measurements of the compression molded plaques were performed in a density gradient column (DGC) according to ASTM D1505-10.

Tensile dogbone specimens were punched from the plaques with a geometry conforming to ISO 527. Tensile tests were conducted on a Zwick Z010 load frame, equipped with a thermostatically-controlled oven, at engineering strain-rates ranging from 10^{-5} to 10^{-1}/s at 65 and 80 °C. The yield strength reported in all cases was the first yield point, and was identified by the intersection of two linear interpolations of the stress–strain curve adjacent to the yield transition. Two tests per condition were conducted for strain-rates 10^{-2} or greater, and only one was conducted for all other conditions.

A coupled analysis of crystallinity and stem length dependence of the yield strength was analyzed using a model considering yield linearly dependent on crystallinity, with this crystallinity dependence also secondarily dependent on stem length. Details of this model are presented in the Results section. The yield strengths at each strain-rate for a given temperature were then fit to a two-term stress-activated Ree–Eyring model,[7] and the parameters of the Ree-Eyring model were also evaluated using a coupled linear model of crystallinity and chain stem length similar to the yield strength. As a note, the test temperatures were chosen to permit a continuous fit to the full Ree–Eyring model for all materials and strain-rates. Lower test temperatures can result in only one observed activation regime in the model.[19]

2.2 | X-ray scattering

X-ray scattering patterns were collected on a Ganesha 300XL instrument from SAXSLAB (now part of Xenocs). A Genix 3D microfocus Cu x-ray source was used to produce x-rays at 50 kV and 0.6 mA, which was passed to an optic to select out the Cu $K\alpha_1$ characteristic x-ray line. The beam was further conditioned by two sets of slits (0.9 x 0.9 mm and 0.8 x 0.8 mm), with the last set having Si scatterless blades. The patterns were collected in transmission mode in vacuum with a sample-to-detector distance of 92.3 and 1042.3 mm and calibrated with a sample of Lanthanum Hexaboride and Silver Behenate for WAXS and SAXS respectively. The detector used was a Dectris Pilatus 300 K vacuum compatible single-photon counting detector, which is fully motorized inside the chamber. The 2D detector images were transmission corrected and reduced to 1D scattering patterns with the SAXSGUI software. There was no orientation detected in any of the cooled samples.

Peak deconvolution was performed in OriginPro 2018 using the Peak Analysis tool. WAXS patterns were fit with two Gaussian curves for the 110 and 200 orthorhombic diffraction peaks and a Pearson VII function for the amorphous halo. The crystallinity is calculated based on the integrated intensity ratio of the crystalline to total area:

$$X_c = \frac{A_{\text{crystalline}}}{A_{\text{crystalline}} + A_{\text{amorphous}}} \tag{1}$$

SAXS showed multiple orders of 00 L lamellar diffraction peaks, which is typical of highly crystalline samples with somewhat regularly spaced lamellae. These were fit with Gaussian curves and the peak-max position was used to calculate the inter-lamellar spacing (L_p). Further, a 1D correlation function, $\Gamma_1(r)$, analysis was performed on the SAXS curves to extract crystal thickness values (l_c), where:

$$\Gamma_1(r) = \frac{1}{Q}\int_0^\infty I(q)q^2\cos(qr)dq \tag{2}$$

with $I(q)$ being the scattered intensity and the scattering invariant, Q, being:

$$Q = \int_0^\infty I(q)q^2dq \tag{3}$$

The crystal thickness, l_c, and other parameters were calculated from Γ_1 according to the procedure in Reference 23. The intensity was extrapolated to 0 and high-q values, as is typical in this analysis, with a Guinier and Porod fit of the intensity, respectively.

$$\text{Guinier}: I(q) = Ae^{Bq^2} \tag{4}$$

$$\text{Porod}: I(q) = B + \frac{K}{q^4} \tag{5}$$

The more important forward extrapolation gave the best results when fit with sharp interfaces (q^{-4}), although

a sigmoidal electron density profile was used, the interface parameter tended to 0 during the fitting process.

The l_c values were assumed to be the larger of the two domains (l_c and l_a) as the WAXS crystallinity values were greater than 50%. The L_p values between SAXS peak fitting and correlation function analysis showed good agreement.

2.3 | Raman spectroscopy

A confocal Raman microscope Alpha 300 R™ (WITec, Inc., Ulm, Germany) equipped with a 785 nm excitation laser was utilized to investigate the compression molded PE plaques described previously. The 785 nm excitation light was focused onto the PE plaques using a 0.25 NA (10x magnification) microscope objective (Zeiss, Oberkochen, Germany) allowing for a greater depth of field. Raman scattered light from the focused 785 nm excitation spot was collected using a 180° backscattering geometry through the same objective and directed through an optical fiber to a spectrometer with a 300 and 1200 g/mm grating. Raman scattered light was dispersed by the spectrometer using a selected grating onto a CCD camera (ANDOR, Belfast, Northern Ireland) to produce a Raman spectrum.

Raman spectra were collected from approximately 625 to 3050 cm^{-1} using the 300 g/mm grating to capture the vibrational regions of interest for determining polyethylene phase morphology. Quantification of polyethylene phase structure was performed similarly to work previously reported by Strobl and Hagedorn.[24] A brief description of the Raman spectral analysis is described, which begins with linear baseline corrections to the C—C stretch (1020–1160 cm^{-1}), CH_2 twist (1250–1350 cm^{-1}), and the CH_2 bend (1390–1510 cm^{-1}) regions of interest in the Raman spectrum (Figure 1A).

The CH_2 twist region was decomposed by peak fitting to yield the areas of the all-trans conformation band at 1295 cm^{-1} and the underlying amorphous conformation band at 1303 cm^{-1} for the purpose of spectral normalization (Figure 1B). Spectral regions of interest (C—C stretch, CH_2 twist, and CH_2 bend) were normalized to the total area of the CH_2 twist region (all-trans and amorphous bands), where the CH_2 twist peak area was corrected to 1. Peak area of the CH_2 twist band was used as an internal standard for normalization due to the integral area of this region being independent of chain conformation as shown by Strobl and Hagedorn.[24] Finally, amorphous contributions from a molten polyethylene spectrum at 160 °C were removed from the spectral regions of interest through a weighted subtraction using primarily amorphous frequencies from 1077 to 1102 cm^{-1} in the C—C

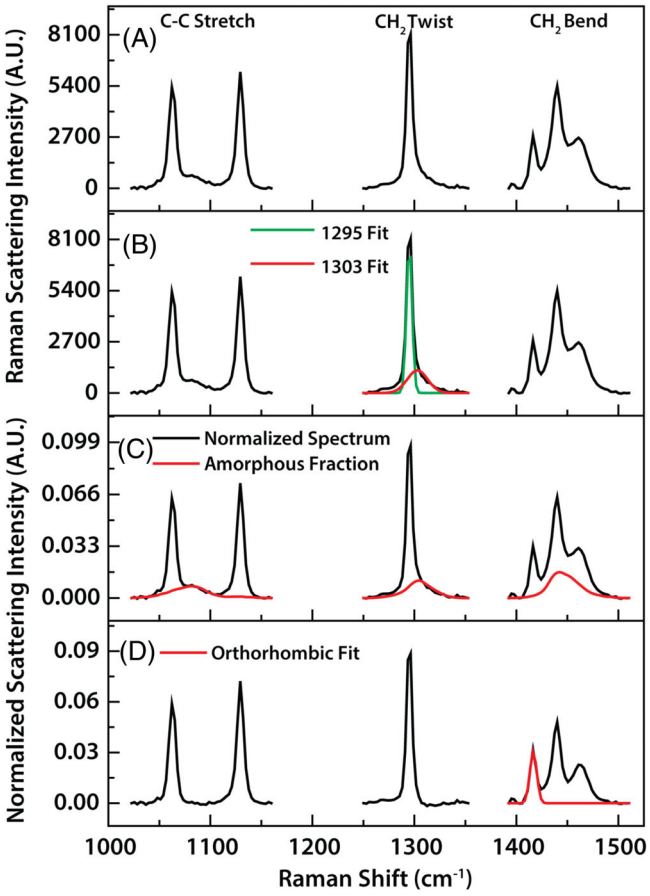

FIGURE 1 (A) Linear baseline corrected C—C stretch, CH_2 twist, and CH_2 bend regions from the Raman spectrum of an ice water quenched HDPE polyethylene plaque. (B) Gaussian fits of the all-trans 1295 cm^{-1} and amorphous 1303 cm^{-1} peaks deconvoluted from the CH_2 twist region. (C) Normalized polyethylene spectrum and weighted amorphous fraction contributions. (D) Gaussian fit of the orthorhombic crystalline peak after weighted subtraction of the amorphous phase

stretch region and frequencies from 1305 to 1349 cm^{-1} in the CH_2 twist region (Figure 1C). Removal of the amorphous phase contributions was performed before fitting of the orthorhombic crystalline peak at 1416 cm^{-1}, which was integrated and ratioed to an experimentally determined constant for quantification of orthorhombic crystallinity (Figure 1D). Orthorhombic crystallinity values from Raman spectroscopy compared reasonably well with X-ray crystallinity values determined from WAXS (Figure 2) on the chrome-catalyzed HDPE, although neither the Raman or X-ray orthorhombic crystallinity values align with crystallinity derived from density.

It was found that the all-trans conformer mass fraction from the CH_2 twist region was more consistent with the theoretical crystallinity derived from the density of the polymer than the orthorhombic crystallinity from Raman spectroscopy, indicating that a significant portion

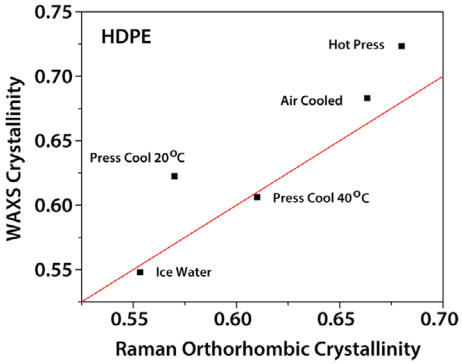

FIGURE 2 Plot of the Raman orthorhombic crystallinity versus the crystallinity determined from WAXS. Line shows parity, indicating that that the WAXS orthorhombic crystallinity is slightly greater than the Raman value, but generally the agreement is close.

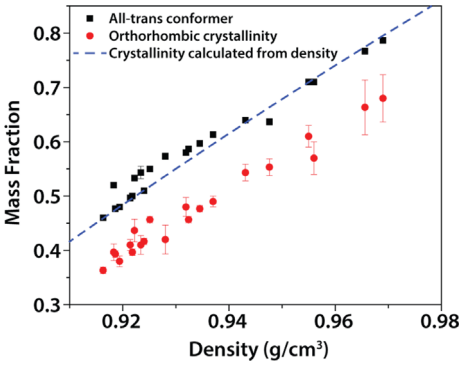

FIGURE 3 Plot of the density gradient column measurements versus the mass fractions of the all-trans conformations and orthorhombic crystallinity obtained from Raman spectroscopy. In addition, a theoretical line of density calculated from the all-trans conformer mass fraction is plotted for comparison, showing good agreement.

of the effective crystallinity is non-orthorhombic. This can be seen in the plot of the all-trans conformer mass fraction and orthorhombic crystallinity versus density in Figure 3, where it is apparent that the all-trans conformer mass fraction and orthorhombic crystallinity have similar slopes, but the all-trans conformer mass fraction is offset from the orthorhombic crystallinity. The density can be calculated assuming a density of 1.003 g/cm^3 for the all-trans conformer mass fraction and 0.850 g/cm^3 for the non-crystalline mass fraction,[5] resulting in good agreement with the density obtained from the density gradient column (DGC) for all samples (Figure 3). For this reason, the all-trans conformer mass fraction was used instead of the orthorhombic mass fraction for crystallinity results presented in this work.

Low wavenumber Raman spectroscopy was used to study the Longitudinal Acoustic Mode (LAM) of

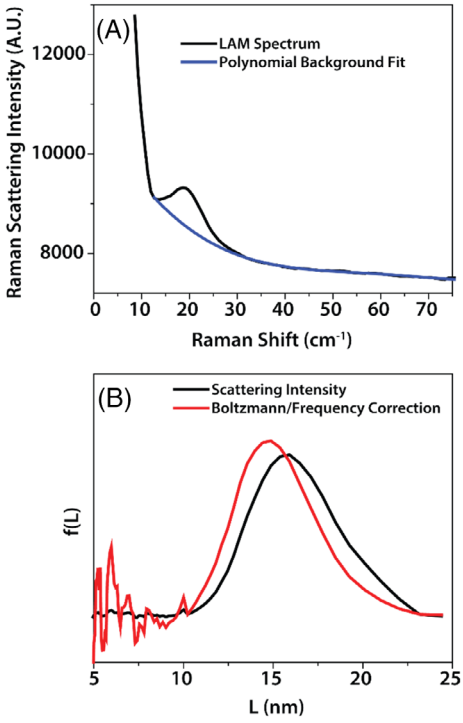

FIGURE 4 (A) LAM spectrum of an ice quenched HDPE polyethylene plaque with a polynomial fit to the background. (B) Background corrected LAM spectrum of an ice quenched HDPE polyethylene plaque before and after the Boltzmann\frequency correction, where the *x*-axis is the ordered sequence length (L). HDPE, high density polyethylenes; LAM, longitudinal acoustic mode.

polyethylene, where spectra were collected over a range of 0–550 cm^{-1} using a 1200 g/mm grating. Methodology for analyzing the LAM spectra of polyethylene was described previously by Snyder[25,26] and employed in this work with some additional data treatment. The fundamental equation used to interpret the LAM spectrum of polyethylene is given below

$$\Delta\nu(\mathrm{LAM}) = \frac{m}{2cL}\left(\frac{E_c}{\rho}\right)^{1/2} \quad (6)$$

where m is the order of the vibrational mode, c is the speed of light, L is the straight-chain segment length, E_c is the elastic modulus, and ρ is the density of the crystalline chains. Equation (6) relates stem length or straight chain segment length L to the Raman spectrum frequency $\Delta\nu$.

Low wavenumber Raman spectra of the LAM-1 mode contained significant noise, which was smoothed using a 5-point moving average filter. After smoothing the spectra, a baseline correction was performed by fitting a polynomial to the excitation laser background (Figure 4A). A linear baseline fit was applied after the polynomial

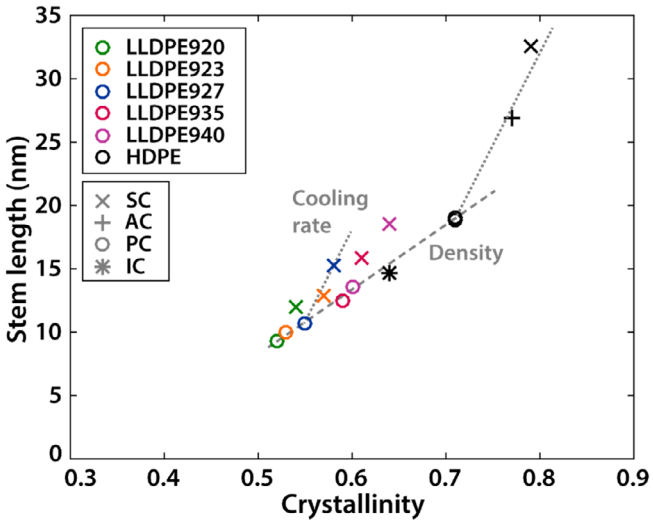

FIGURE 5 Crystallinity (all-trans conformer mass fraction) and chain stem length were varied independently through thermal treatment and comonomer concentration. The shape of the symbol is used to indicate the thermal treatment and color to denote the polymer. Trend lines are added to differentiate the effect of cooling rate (short dashes) from nominal density (long dashes).

background subtraction to define the beginning and end points of the distribution, which was then normalized to an area of 1.

Following the removal of the polynomial background fit and linear correction, a Boltzmann temperature and frequency correction were applied to the observed Raman scattering intensity to obtain the straight chain segment length distribution as can be seen in Figure 4B, which is normalized to an area of 1.[25,26] The ordered chain length distribution is related to the observed Raman scattering intensity by the following equation:

$$f(L) \propto \left[1 - \exp\left(-\frac{hc\Delta\bar{\nu}}{kT}\right)\right](\Delta\bar{\nu})^2 I_{\nu}^{obs} \tag{7}$$

where I_{ν}^{obs} is the observed scattering intensity at frequency ν, $\left[1-\exp\left(-\frac{hc\Delta\bar{\nu}}{kT}\right)\right]$ is the Boltzmann correction for temperature, and $(\Delta\bar{\nu})^2$ is a frequency correction for the distribution $f(L)$ in units of length L.

3 | RESULTS

3.1 | Morphology

Crystallinity and stem length were controllably varied by utilizing short-chain branching in addition to processing conditions (Figure 5). Taking the quenched materials (minimum stem length) for each nominal density, one obtains a baseline "density effect" correlation between stem length and crystallinity. Fortunately, considering the case of a specific resin, the set of various quench conditions results in a correlation between stem length and crystallinity that is not parallel to the composition baseline correlation. In this way, we were able to independently vary stem length and crystallinity such that their influence on plasticity can be assessed separately and simultaneously.

3.2 | Coupled crystallinity and stem length analysis of yield

The complete deformation response at 65 °C up to failure or 60% strain is shown in Figure 6 for HDPE SC and LLDPE940 SC. A peak stress at yield is evident for HDPE, while for lower densities the peak is marginal or there is no peak at yield. The general lack of a peak stress at yield drives the need to use a bilinear extrapolation to determine the yield strength. A second yield transition is also evident in the lower strain-rate tests for the LLDPE940 (and other LLDPEs), just prior to the onset of necking.

Figure 7 presents the yield strength as a function of crystallinity for each applied strain-rate, $\dot{\varepsilon}$; it is clear that for each strain rate, the yield strength depends approximately linearly on crystallinity, ξ, within the range of strain rates considered.

The clear linear dependence of the yield strength on crystallinity at each strain-rate motivates a linear model function of crystallinity, where it can be represented as a crystalline yield function A that depends on strain-rate, $\dot{\varepsilon}$, and chain stem length, L, and is linear with the crystallinity, ξ, in addition to a second non-crystalline yield function B that depends only on strain-rate and is linear with the non-crystalline fraction, $(1-\xi)$:

$$\sigma_y(\dot{\varepsilon},\xi,L) = A(\dot{\varepsilon},L)\xi + B(\dot{\varepsilon})(1-\xi) \tag{8}$$

The crystalline yield function A is itself considered linear in stem length,

$$A(\dot{\varepsilon},L) = A_1(\dot{\varepsilon})L + A_2(\dot{\varepsilon}) \tag{9}$$

which allows for the modeling of the yield strength as primarily linearly dependent on crystallinity through A_2 and B, but secondarily linearly dependent on stem length through A_1.

Thus, for a certain fixed strain-rate, we can rewrite the expanded form of Equations (8) and (9),

$$\sigma_y = \xi(A_2 - B) + \xi L A_1 + B \tag{10}$$

Pulling the crystallinity and constant functions to the left-hand side, we obtain a linear function of the stem

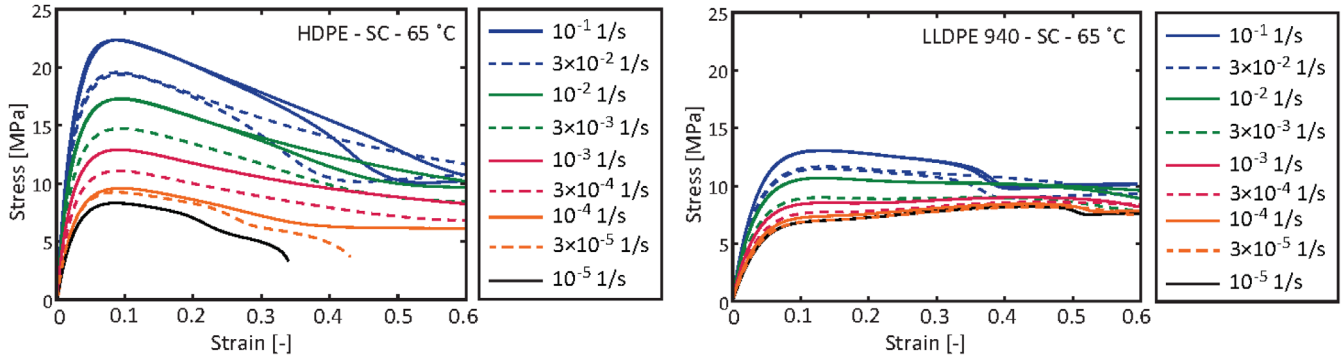

FIGURE 6 Tensile deformation response of high density polyethylenes SC and LLDPE940 SC at 65 °C and strain-rates from 10^{-5} to 10^{-1}/s. the first yield transition (around 5% strain) is used for the present work, and is identified by a bilinear extrapolation of the stress–strain curve about the transition.

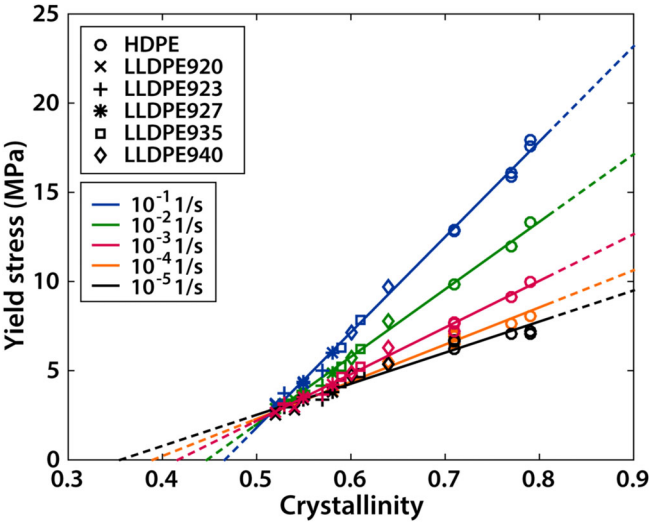

FIGURE 7 Dependence of yield strength on crystallinity for each material, strain-rate, at 80 °C

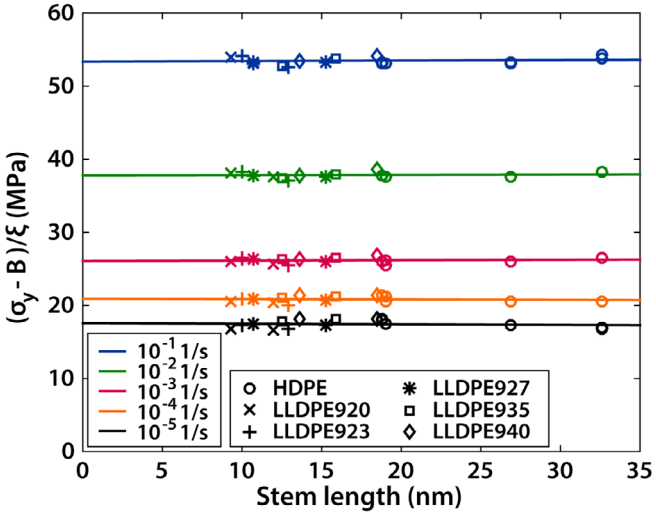

FIGURE 8 The secondary stem length dependence of the yield function is negligible for all conditions

length (Equation 11). This allows the analysis of data fit to Equation (8) in Figure (6) to be analyzed for a secondary dependence in stem length.

$$\frac{\sigma_y - B}{\xi} = (A_2 - B) + LA_1 \tag{11}$$

After fitting the yield strength data to Equation (8) for each strain-rate (Figure 7) plotting according to Equation (11) yields a series of linear interpolations of the secondary stem length dependence of the yield strength for various constant strain-rates (Figure 8). It is clear from Figure 8 that the secondary stem length dependence is negligible. This demonstrates that crystallinity alone is a sufficient morphological determinant of the strain-rate and temperature-dependent yield strength.

3.3 | Coupled crystallinity and stem length analysis of the Ree–Eyring model parameters

The preceding analysis showed the yield strength is dependent only on crystallinity when both the strain-rate and temperature are fixed, but for all the tested strain-rates and temperatures tested. A unified model that predicts the strain-rate and temperature effects on yield with a single set of crystallinity and stem length-dependent parameters would be more conclusive. Thus, the Ree–Eyring activated rate model was employed and tested for crystallinity and chain stem length dependence of its free parameters.

The Ree–Eyring activated rate model of yield considers two activated-rate dissipative processes in parallel, with the second term corresponding to the higher strain-rate activated component (Figure 9).

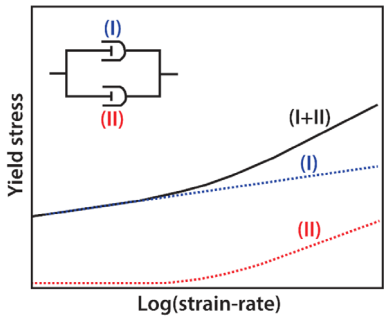

FIGURE 9 The Ree–Eyring model considers two activated-rate processes in parallel with the second system by convention activating at higher strain-rates

The Ree–Eyring Equation (7),

$$\sigma_y = \frac{kT}{V_I^*}\sinh^{-1}\left(\frac{\dot{\varepsilon}}{\dot{\varepsilon}_{0,I}\exp\left(-\Delta U_I/kT\right)}\right) + \frac{kT}{V_{II}^*}\sinh^{-1}\left(\frac{\dot{\varepsilon}}{\dot{\varepsilon}_{0,II}\exp\left(-\Delta U_{II}/kT\right)}\right) \quad (12)$$

was fit to the yield strength data with the activation volumes (Equation 13) and combined rate constants (Equations 14 and 15) considered as a linear function of crystallinity and stem length, similarly to the above analysis of the yield strength. Yield strength measurements were plotted against log(strain-rate) in the typical manner for stress-activation plots, and regression fits were obtained for each curve according to the two-process Ree–Eyring model (Figure 10). In the fitting procedure, the activation volume for the first process, V_I^*, was assumed to be constant, and taken the value determined by Kanters et al. for HDPE.[6] The reason for this was that the range of strain-rate available for calibrating the first process alone was limited as a result of annealing effects: the long experimental times at low strain-rates lead, at elevated temperature, to microstructural changes that increase the yield stress during the experiment. This was verified by performing annealing treatments with extended exposure times, after which the yield stress at a strain-rate of 10^{-3} s^{-1} was observed to increase markedly. Hence the data at strain-rates lower than 10^{-4} s^{-1}, indicated by the gray markers in Figure 10, were omitted from the analysis, though the effect only appears significant for the lower crystallinity materials. Within the remaining range of strain-rates for Process I, the activation volume could, within experimental error, be assumed as constant.

The linear modeling of the yield kinetics was conducted as before, but for the free parameters in the Ree–Eyring model. Thus, for a given strain-rate and temperature, we have the activation volume function, where C_1, C_2, and D are constants,

$$V^* = \xi(C_2 - D) + \xi L C_1 + D \quad (13)$$

and the combined rate constant for each term is collapsed, such that the rate constant $\dot{\varepsilon}_0$ and Arrhenius activation term are combined into a single parameter, F:

$$F = \log\left(\dot{\varepsilon}_0 \exp\left(-\frac{\Delta U}{kT}\right)\right) \quad (14)$$

The combined rate constant F is also treated as a linear function of crystallinity and stem length similar to above, where G_1, G_2, and H are fit constants.

$$F = \xi(G_2 - H) + \xi L G_1 + H. \quad (15)$$

The crystallinity and stem length dependent activation volumes and combined rate constants were simultaneously fit to the continuous yield data as seen in Figure 10, and the results for the individual parameter dependences on crystallinity are shown in Figures 11 and 12. Process I activation volume is held constant and is shown gray to indicate that it is not allowed to vary in the fitting process. Additionally, data from the two lowest density materials are omitted from Figure 11 as the fit for V_{II}^* had a low confidence.

The activation volume and combined rate constant are both linear with crystallinity, which validates the assumed form in the model. The first term activation volume is assumed independent of crystallinity and the second term is linear and inversely correlated with crystallinity. The combined rate constant for Process I is inversely correlated with crystallinity, as is the Process II combined rate constant, but weakly so.

Following the same procedure as for the yield strength, the secondary stem length dependence of the activation volumes and combined rate constants is seen to be negligible (Figures 13 and 14). Thus, it has been demonstrated that the yield kinetics and their mechanical and thermal activation over a wide range of quasi-static strain-rates at elevated temperature are linearly dependent on crystallinity and independent of chain stem length in the crystal lamellae.

4 | DISCUSSION

The results of this work strongly conclude that the yield kinetics of lamellar polyethylene at elevated temperatures is dependent on crystallinity and not on crystal chain stem length. The set of polyethylene homopolymer and copolymers and solidification conditions utilized in this work achieved some independence of crystallinity from crystal thickness such that these two morphological

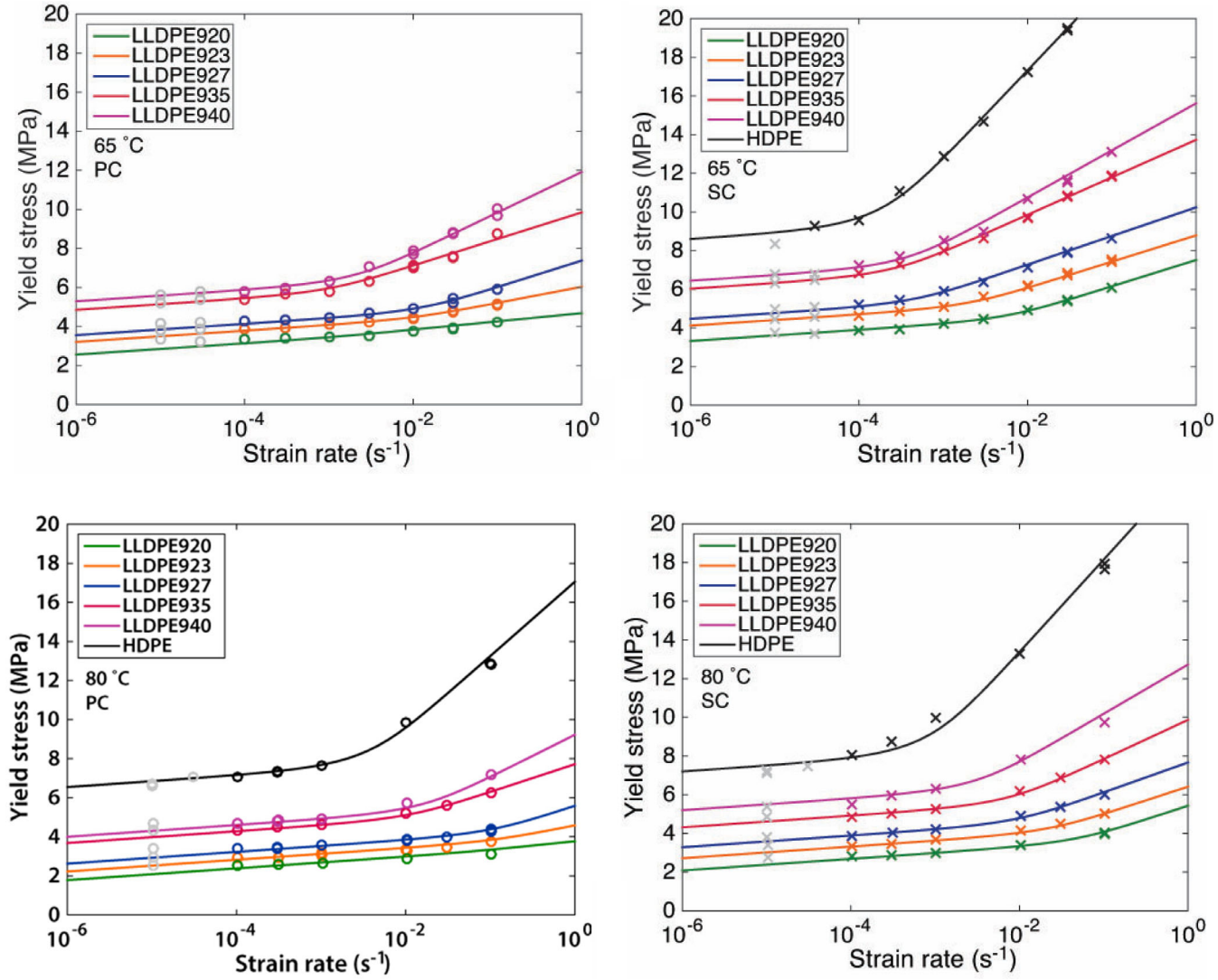

FIGURE 10 Ree–Eyring fits to the experimental data for both test temperatures and heat treatments. All parameters for the model as a function of crystallinity and stem length (Equations 13–15) were simultaneously calibrated. Points in gray are neglected from the fit due to microstructural annealing over long duration experiments.

attributes could be disentangled in a two-factor analysis. The experimental results clearly indicate that the yield strength and its activated rate behavior are linearly dependent on crystallinity for a given strain-rate and temperature, and that any secondary effect of chain stem length is negligible. It is worth noting that models of the expected chain stem length dependence of yield kinetics from dislocation nucleation models are nonlinear—but the results of this work unambiguously reject any stem length dependence of the yield kinetics secondary to the crystallinity dependence.

From a composite theory perspective, it is expected that the yield strength and elastic moduli depend on crystallinity, regardless of any effect of chain stem length. Conversely, there is little case for plasticity to depend on chain stem length only and not crystallinity, as any crystal thickness dependence must clearly operate on a crystalline component of the response, and therefore depend on the degree of crystallinity. The strong correlation of crystallinity and crystal thickness has previously obscured this point. Nevertheless, there is a substantial amount of literature reporting yield strength primarily depending on chain stem length, and this deserves to be revisited in light of the present work. Returning to the work of Argon and coworkers,[13] a saturation in the yield strength with reported lamellar thickness was reported and attributed to the activation of dislocation loops. However, when their previously reported crystallinity values for these data[27] are plotted instead against their reported lamellar thickness measurements (as measured by DSC), one sees that the saturation of the yield stress occurring is due to the crystallinity nearing a maximum value and

the lamellae approaching the equilibrium crystallization condition where crystal thickness diverges according to the Gibbs–Thompson equation (Figure 15). Their yield strength data collapse to a linear function of crystallinity, and thus there is no contradiction between their reported data and the results of the present work.

This work utilized crystallinity and chain stem lengths obtained from Raman spectroscopy, similar to previous works,[2–4] and these results were compared to values obtained from SAXS, WAXS, and DSC. The Raman all-trans conformer mass fraction produced accurate predictions of overall density when compared to density gradient column values (and therefore conventional crystallinity measures—Figure 3), while the orthorhombic conformer mass fraction underpredicted density. The orthorhombic crystallinity obtained by WAXS was slightly greater than the Raman orthorhombic mass fraction, but still significantly less than the all-trans conformer mass fraction. Further, the longitudinal acoustic mode measure of chain stem length has been shown to be an accurate measure of crystal thickness by comparison to estimates from small-angle and wide-angle X-ray scattering (Figures 2 and 3), also for example Reference 24. This is an important note, as significant

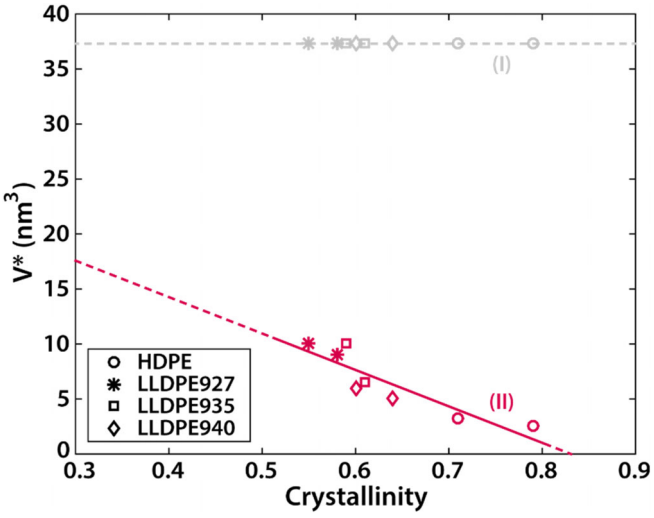

FIGURE 11 Activation volume for Process II in the Ree–Eyring model for all materials is linear with crystallinity. The activation volume for Process I was assumed constant from Reference 6 and is shown in gray.

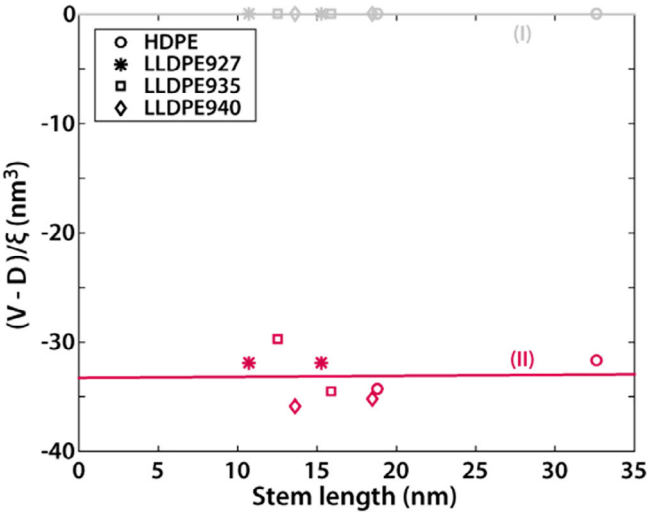

FIGURE 13 The secondary dependence of the activation volume of Process II on chain stem length is negligible. Process I activation volume is assumed constant (grayed).

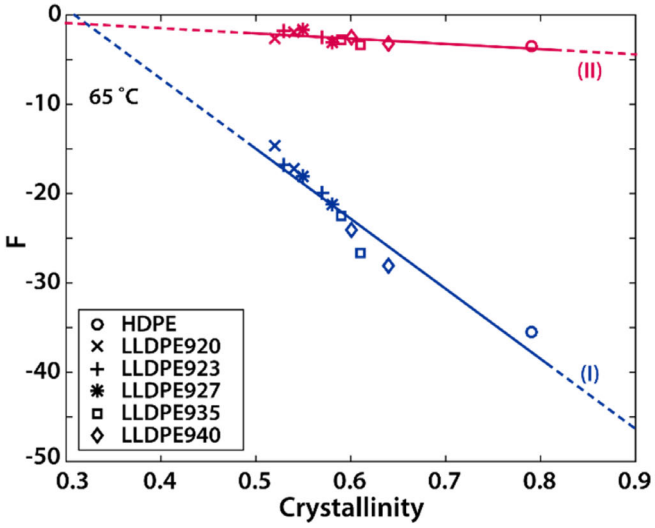

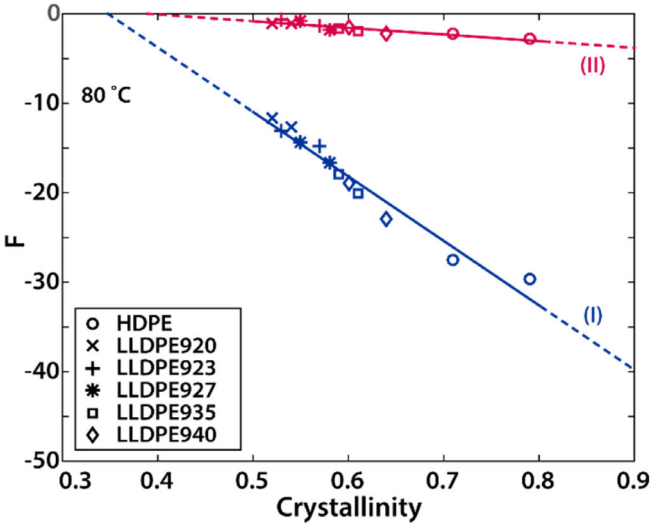

FIGURE 12 Combined rate constants for both Ree–Eyring processes are linear with crystallinity for all materials, shown at both 65 and 80 °C

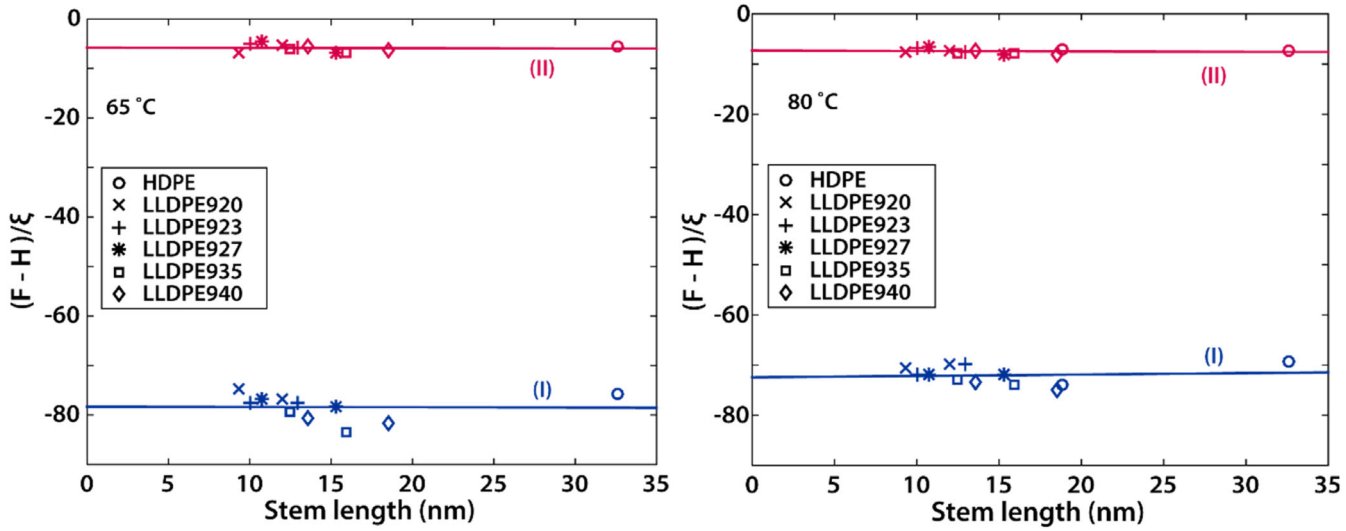

FIGURE 14 The secondary dependence of the combined rate constants on chain stem length is negligible. Data are shown for both 65 and 80 °C.

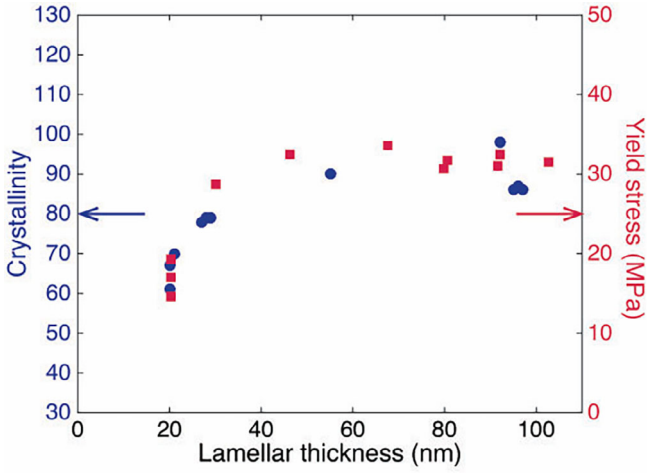

FIGURE 15 (a) Crystallinity reported by Kazmierczak et al.[27] show a saturation of crystallinity with increasing lamellar thickness, commensurate with expectations for near-equilibrium crystallization. Replotting the yield results onto a second axis for these data by Argon et al.[13] show an identical trend. The overlap of these trends reveals a linear dependence of yield stress on crystallinity that went unreported in their work.

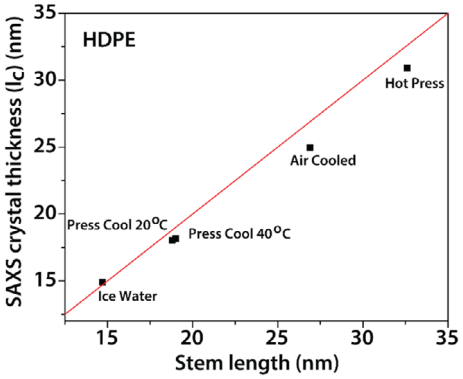

FIGURE 16 Plot of the stem length from Raman longitudinal acoustic mode versus the crystal thickness determined from the SAXS 1D correlation function (l_c). Parity is shown with a line, indicating that the SAXS crystal thickness lags the stem length marginally.

divergence arises between LAM stem length and crystal thickness obtained from the Gibbs-Thompson relationship from DSC for thicker crystals with melting temperatures approaching the equilibrium limit.[28] Many of the previous studies on this subject depend on crystal thickness obtained from the Gibbs-Thompson relation for high crystallinity. For these reasons, only Raman spectroscopy results were used for microstructural characterization so that the analysis would consistent with conventional measures of crystallinity (i.e., density), internally consistent, and independent of concerns arising with indirect measures of chain stem length from SAXS/WAXS or DSC.

Ordered chain length (stem length) derived from low wavenumber Raman spectroscopy of the LAM-1 mode for the variously quenched HDPE samples were compared against X-ray scattering results for the crystal thickness, l_c, which can be seen in Figure 16. Average stem length values from the Raman data were consistent with crystal thickness values determined from SAXS using the 1D correlation function, but begin to differ at longer chain stem lengths determined from the Raman LAM analysis, though the difference is marginal. Overall, these data draw the interpretation that the chain stem is oriented in the direction of the 1D correlation, that is,

normal to the surface of the crystal, with minimal chain tilt. The possible complication of an unknown chain tilt was the motivation to avoid using SAXS to determine the chain stem length, being the operative crystalline dimension for determining slip kinetics, but the comparison of the correlation coefficient crystal thickness and stem length seem to render this concern moot, at least for the HDPE samples compared in the present work.

The dislocation-mediated plasticity literature clearly indicates that crystal slip is expected to be chain stem length dependent, owing to the nucleation of through-thickness screw dislocations as the rate-limiting mechanism.[9,11–13] The conclusion of this work, that the yield kinetics in lamellar polyethylene are independent of chain stem length, is entirely experimentally determined without a clear mechanistic argument, and therefore deserves some further theoretical consideration. First, it should be noted that Young's model[9] and those who expanded on it focused only on the lowest energy slip system, that is, screw dislocation-mediated chain slip, and did not examine the kinetics of other systems. The polyethylene crystal plasticity literature has considered at least six systems simultaneously active, and has shown both chain slip and transverse slip to be active at the first yield point.[19] Transverse slip is likely accommodated by either chain stem edge dislocations (or loops) or transverse screw dislocations, which would not be expected to have a stem length dependence. All of these systems are expected to have a considerably higher activation energy than screw-mediated chain slip.[10] Both Young and Argon discussed the nucleation of dislocation half-loops as thickness-independent, though the latter proposed this as an explanation for the apparent saturation of yield strength dependence at large crystal thickness. It may be that nucleation of dislocation loops are the dominant mechanism even for relatively thin crystals, so long as the chain stem length exceeds 20 Burgers vectors.[13] In an alternative approach, Brooks et al. conducted an analysis of the expected temperature dependence of the yield strength compared to a theory of kink pair nucleation.[11] They reported that yield in polyethylene followed the expected dependence on temperature (normalized by shear modulus) only substantially below room temperature (−20 to −40 °C), and at higher temperatures they concluded that yield is not nucleation dominated, but rather is dislocation propagation limited. Indeed, in his original work, Young anticipated the possibility that dislocation-mediated slip in polyethylene is rate-limited by the Peierls stress for driving dislocations through the lattice, and estimated that the process could be primarily limited by the Peierls stress for the low-energy chain slip process he considered.[9] Following this interpretation for the present work, it is consistent that slip activation in polyethylene above room temperature is dominated by the Peierls stress, which is expected in general to be chain stem length independent.[29] This perspective on slip not being limited by dislocation nucleation at elevated temperatures is compatible with the observation of widespread thermal activation of chain stem motions in the alpha process under those conditions. Alpha process activation may not be distinguishable from the nucleation of screw dislocation line segments for the chain slip process, as both involve the spontaneous nucleation of twisting or corkscrewing motions of the chain stem in the lattice along the stem axis.[29–31] More work needs to be conducted along the lines of the present work to investigate whether slip kinetics in polyethylene are also chain stem length-independent below −20 °C, or whether dislocation nucleation dominates in that regime, with a concomitant emergent stem length dependence only active under those conditions.

The foregoing literature discussed here mainly concerned the yielding behavior of polyethylene, which is to say the apparent onset of plastic deformation. Polyethylene is often observed to have two distinct yield points; the literature generally holds that the first yield process is determined by a dislocation-mediated fine slip process, while the second yield involves coarse non-crystallographic slip and the fragmentation of crystals into mosaic blocks.[32,33] The present work concerns only measurements at the first yield point—in this paper we do not invalidate the notion of fine crystallographic slip during first yield, but rather call into question whether the kinetics of first yield depend on the kinetics of screw dislocation nucleation, as described by Young and others. Notably, the critical strains corresponding to characteristic points of the stress–strain curve were observed to be independent of crystallite thickness for s-PP.[34] While there has been work investigating microstructural mechanisms underlying plastic deformation at strains beyond the first yield, an investigation of the simultaneous crystallinity and chain stem length dependence of such large plastic strains remains a subject for future work.

The Ree–Eyring activation volumes and combined rate constants showed stem length independence. However, it could be that either the rate constants or activation energies, when fit individually, are stem length dependent. The temperature range tested in this work was insufficiently broad to allow a satisfactory fit to these parameters individually, and hence, only combined rate constants are reported. However, it seems unlikely that the activation energy and rate constant parameters could be stem length dependent in an exactly reciprocal manner such that the combined rate constant shows the stem length independence that was observed. Thus, we are

confident that the results of this work satisfactorily demonstrate that the activated rate yield kinetics of polyethylene at elevated temperature are independent of chain stem length.

The results of this work are good news for micromechanical modeling of polyethylene in the regime of yield kinetics explored in this work, as a crystal plasticity model calibrated to a given microstructure can be expected to apply to a different microstructure without having to recalibrate the slip kinetics for crystal thickness or chain stem tilt. However, it remains to be established whether first yield slip kinetics in other semicrystalline polymers are chain stem length independent.

5 | CONCLUSIONS

This work employed a model set of polyethylene lamellar microstructures with a range of decorrelated chain stem lengths and crystallinity, which allowed these parameters to be analyzed independently. It was shown that the yield strength (first yield point) over a wide range of strain-rates is linearly dependent on crystallinity and that there is no secondary dependence on the crystal chain stem length. Further, the activation volume and combined rate constant likewise showed linear dependence on crystallinity and no dependence on chain stem length. The crystallinity dependence is not surprising from the perspective of composite theory, though the lack of a secondary stem length dependence was not expected. This observation of stem length independence differs with much of the polyethylene plasticity modeling literature, which is based on the rate-limiting step being the nucleation of screw dislocations in the crystal with a chain stem-dependent activation energy. The results of this work cast doubt on screw dislocation nucleation being the dominant mechanism for yield kinetics, at least under the elevated temperature conditions tested in the present work. Notably, yield strength measurements presented in support of the dislocation nucleation model also were shown to nevertheless demonstrate a linear dependence on crystallinity without need to appeal to chain stem length. Alternative explanations of this chain stem length-independent plasticity include the nucleation of dislocation half loops or a Peierls stress that is greater than the dislocation nucleation stress. Further deformation experiments should be conducted to evaluate whether yield at low temperatures is also stem length independent, or rather varies with stem length and so may be dislocation nucleation dominated under those conditions.

ACKNOWLEDGEMENTS

This work was funded by ExxonMobil Research and Engineering Company.

ORCID

Jevan Furmanski https://orcid.org/0000-0002-1630-5285

REFERENCES

[1] R. W. Truss, P. L. Clarke, R. A. Duckett, I. M. Ward, *J. Polym. Sci. Part B: Polym. Phys.* **1984**, *22*, 191.
[2] R. Popli, L. Mandelkern, *J. Polym. Sci. Part B: Polym. Phys.* **1987**, *25*, 441.
[3] A. J. Peacock, L. Mandelkern, *J. Polym. Sci. Part B: Polym. Phys.* **1990**, *28*, 1917.
[4] M. A. Kennedy, A. J. Peacock, L. Mandelkern, *Macromol* **1994**, *27*, 5297.
[5] B. Crist, C. J. Fisher, P. R. Howard, *Macromol* **1989**, *22*, 1709.
[6] M. J. W. Kanters, K. Remerie, L. E. Govaert, *Polym. Eng. Sci.* **2016**, *56*, 676.
[7] T. Ree, H. Eyring, *J. App. Phys.* **1955**, *26*, 793.
[8] H. Eyring, *J. Chem. Phys.* **1936**, *4*, 283.
[9] R. G. Young, A. Dislocation, *Philos. Mag.* **1974**, *30*, 85.
[10] L. G. Shadrake, F. Guiu, *Philos. Mag.* **1976**, *34*, 565.
[11] N. W. J. Brooks, R. A. Duckett, I. M. Ward, *J. Polym. Sci. Part B: Polym. Phys.* **1998**, *36*, 2177.
[12] N. W. J. Brooks, M. Mukhtar, *Polymer* **2000**, *41*, 1475.
[13] A. S. Argon, A. Galeski, T. Kazmierczak, *Polymer* **2005**, *46*, 11798.
[14] A. Keller, S. Sawada, *Die Makromolekulare Chemie* **1964**, *74*, 190.
[15] D. C. Bassett, A. M. Hodge, *Proc R Soc Lond A* **1981**, *377*, 25.
[16] S. Gautam, S. Balijepalli, G. C. Rutledge, *Macromolecules* **2000**, *33*, 9136.
[17] B. J. Lee, D. M. Parks, S. Ahzi, *J. Mech. Phys. Solids* **1993**, *41*, 1651.
[18] S. Nikolov, R. A. Lebensohn, D. Raabe, *J. Mech. Phys. Solids* **2006**, *54*, 1350.
[19] A. Sedighiamiri, L. E. Govaert, M. J. W. Kanters, J. A. W. van Dommelen, *J. Polym. Sci. Part B: Polym. Phys.* **2012**, *50*, 1664.
[20] J. A. W. van Dommelen, D. M. Parks, M. C. Boyce, W. A. M. Brekelmans, F. P. T. Baaijens, *J. Mech. Phys. Solids* **2003**, *51*, 519.
[21] S. M. Mirkhalaf, J. A. W. van Dommelen, L. E. Govaert, J. Furmanski, M. G. D. Geers, *J. Polym. Sci. Part B: Polym. Phys.* **2019**, *57*, 378.
[22] E. V. Bensason, S. Stepanov, A. Chum, A. Hiltner, E. Baer, *Macromolecules* **1997**, *30*, 2436.
[23] A. J. Ryan, *Fibre Diffract Rev* **1994**, *3*, 25.
[24] G. R. Strobl, W. Hagedorn, *J. Polym. Sci. Polym. Phys. Ed.* **1978**, *16*, 1181.
[25] R. G. Synder, S. J. Krause, J. R. Scherer, *J. Polym. Sci. Polym. Phys. Ed.* **1978**, *16*, 1593.
[26] R. G. Synder, J. R. Scherer, *J. Polym. Sci. Polym. Phys. Ed.* **1980**, *18*, 421.

[27] T. Kazmierczak, A. Galeski, A. S. Argon, *Polymer* **2005**, *46*, 8926.
[28] Y. Furushima, M. Nakada, M. Murakami, T. Yamane, A. Toda, C. Schick, *Macromolecules* **2015**, *48*, 8831.
[29] J. M. Peterson, *J. Appl. Phys.* **1968**, *39*, 4920.
[30] S. Nikolov, D. Raabe, *Polymer* **2006**, *47*, 1696.
[31] M. Mansfield, R. H. Boyd, *J. Polym. Sci., Polym. Phys. Ed.* **1978**, *16*, 1227.
[32] L. Lin, A. S. Argon, *J. Mater. Sci.* **1994**, *29*, 294.
[33] R. Hiss, S. Hobeika, C. Lynn, G. Strobl, *Macromolecules* **1999**, *32*, 4390.
[34] Y. Men, G. Strobl, *J. Macromol. Sci.* **2001**, *40*, 775.

How to cite this article: J. Furmanski, L. Govaert, J. Schaefer, J. A. Throckmorton, J. A. W. van Dommelen, *J. Polym. Sci.* **2022**, *60*(22), 3085. https://doi.org/10.1002/pol.20220265